Zhan et al. *Zool. Res.* 2024, 45(6): 1175−1187
https://doi.org/10.24272/j.issn.2095-8137.2024.219
https://cstr.cn/32248.14.zr.2024.219

ZR | Zoological Research

Article Open Access

IDH2 and GLUD1 depletion arrests embryonic development through an H4K20me3 epigenetic barrier in porcine parthenogenetic embryos

Cheng-Lin Zhan[1,#], Qin-Yue Lu[1,#], Song-Hee Lee[1], Xiao-Han Li[1], Ji-Dam Kim[1], Gyu-Hyun Lee[1], Jae-Min Sim[1], Hyeon-Ji Song[1], Ying-Yan Jin[1], Xiang-Shun Cui[1,*]

[1] *Department of Animal Science*, *Chungbuk National University*, *Cheongju*, *Chungbuk* 28644, *Republic of Korea*

ABSTRACT

Isocitrate dehydrogenase 2 (IDH2) and glutamate dehydrogenase 1 (GLUD1) are key enzymes involved in the production of α-ketoglutarate (α-KG), a metabolite central to the tricarboxylic acid cycle and glutamine metabolism. In this study, we investigated the impact of IDH2 and GLUD1 on early porcine embryonic development following *IDH2* and *GLUD1* knockdown (KD) via double-stranded RNA (dsRNA) microinjection. Results showed that KD reduced α-KG levels, leading to delayed embryonic development, decreased blastocyst formation, increased apoptosis, reduced blastomere proliferation, and pluripotency. Additionally, *IDH2* and *GLUD1* KD induced abnormally high levels of trimethylation of lysine 20 of histone H4 (H4K20me3) at the 4-cell stage, likely resulting in transcriptional repression of embryonic genome activation (EGA)-related genes. Notably, KD of lysine methyltransferase 5C (*KMT5C*) and supplementation with exogenous α-KG reduced H4K20me3 expression and partially rescued these defects, suggesting a critical role of *IDH2* and *GLUD1* in the epigenetic regulation and proper development of porcine embryos. Overall, this study highlights the significance of *IDH2* and *GLUD1* in maintaining normal embryonic development through their influence on α-KG production and subsequent epigenetic modifications.

Keywords: A-ketoglutarate; H4K20me3; IDH2; GLUD1; Embryonic development

INTRODUCTION

Mammalian life begins with the fertilization of an oocyte by a sperm, leading to the formation of a blastocyst (BL) during the preimplantation phase. This stage encompasses critical biological events, including embryonic genome activation (EGA), which precedes the first cell-fate decisions and lineage-specific differentiation (Sozen et al., 2014; Zernicka-Goetz et al., 2009). Correct reprogramming of epigenetic modifications during this process is essential for successful preimplantation development. Parthenogenetic activation (PA) and somatic cell nuclear transfer (SCNT) embryos typically undergo asynchronous epigenetic reprogramming compared to *in vitro* fertilization (IVF) embryos, which significantly affects the SCNT success rate (Liu et al., 2016). Abnormal reprogramming of histone H3 lysine 9 trimethylation (H3K9me3) and lysine 27 trimethylation (H3K27me3) has been identified as an epigenetic barrier to SCNT embryo development in mice (Antony et al., 2013; Wang et al., 2020) and cattle (Zhou et al., 2019).

Trimethylation of lysine 20 of histone H4 (H4K20me3) is an essential post-translational modification involved in epigenetic regulation. It serves as a hallmark of silenced heterochromatin and plays a key role in maintaining genomic integrity (Jørgensen et al., 2013). The regulation of H4K20me3 is dynamically controlled by lysine methyltransferase 5C (KMT5C, Suv4-20h2 in mice) (Balakrishnan & Milavetz, 2010; Qian & Zhou, 2006) and the histone demethylase homolog of RAD23 protein (Cao et al., 2020). H4K20me3 levels fluctuate dynamically during mouse embryogenesis, with lower levels during EGA at the 2-cell (2C) stage and higher levels during PA and SCNT embryos compared to IVF embryos (Liu et al., 2024). Notably, Suv4- 20h2 knockdown (KD) enhances the efficiency of mouse cloning (Liu et al., 2024). These observations suggest that H4K20me3 reprogramming is an integral process for regulating embryonic development.

Cellular metabolism underpins all biological processes, with proper metabolic balance essential for preimplantation embryonic development. Isocitrate dehydrogenase (IDH2) and glutamate dehydrogenase 1 (GLUD1) are key enzymes involved in the production of α-ketoglutarate (α-KG), a central metabolite in the tricarboxylic acid cycle and glutamine

Received: 27 June 2024; Accepted: 03 September 2024; Online: 04 September 2024

Foundation items: This work was supported by the National Research Foundation (NRF) of Korea grant funded by the Korean government (MSIT) (2022R1A2C300769), Republic of Korea

#Authors contributed equally to this work

*Corresponding author, E-mail: xscui@cbnu.ac.kr

metabolism. Research on IDH2 has primarily focused on its mutations, which produce the metabolite (R)-2-hydroxyglutarate (R-2-HG). This metabolite competes with α-KG, leading to disruptions in cellular metabolism and the development of various cancers (Figueroa et al., 2010; Sunthankar et al., 2022). In leukemia, IDH2 mutations are associated with global DNA hypermethylation and specific hypermethylation signatures (Figueroa et al., 2010). R-2-HG, produced by mutated IDH2, inhibits KDM5 histone lysine demethylases, highlighting its important role in maintaining epigenetic stability. In contrast, GLUD1 participates in epigenetic modification by catalyzing the production of α-KG. Degradation of GLUD1 reduces intracellular α-KG levels, leading to increased methylation of H3K9me3 and H3K27me3 (Shao et al., 2021).

In addition to its metabolic functions, α-KG, produced by IDH2 and GLUD1, acts as a cofactor for α-KG-dependent dioxygenases, such as JmjC-domain containing histone demethylases (JHDMs) and ten-eleven translocation (TET) enzymes, which play critical roles in regulating the epigenetic landscape (Kaelin & McKnight, 2013). Supporting this, α-KG supplementation has been shown to positively affect mouse embryonic development by modulating mitochondrial function, slightly reducing adenosine triphosphate (ATP) production, and activating TET enzymes to promote DNA demethylation (Zhang et al., 2019). Furthermore, increased intracellular α-KG levels or elevated α-KG-to-succinate ratios have been found to favor self-renewal in naïve mouse embryonic stem cells (Carey et al., 2015). These findings demonstrate that dynamic fluctuations in α-KG levels are essential for maintaining epigenetic stability and driving differentiation.

In the present study, we silenced IDH2 and GLUD1 in porcine PA embryos via microinjection of IDH2 and GLUD1 double-stranded RNA (dsRNA) and assessed the impact of KD on embryonic development, BL quality, and inner cell mass (ICM) ratio. Moreover, given that α-KG serves as a cofactor of RAD23, we examined changes in the expression of intracellular H4K20me3. Results revealed abnormally high expression of H4K20me3 in embryos with IDH2 and GLUD1 KD, which likely impaired EGA and disrupted ICM differentiation.

MATERIALS AND METHODS

Reagents

All reagents were purchased from Millipore Sigma (USA) unless stated otherwise.

Ethical approval

This study was performed following the guidelines of the Institutional Animal Care and Use Committee of Chungbuk National University Laboratory Animal Center, Cheongju, Republic of Korea. All experimental procedures were examined and approved by the Animal Research Committee at the National Institute of Animal Science (NIAS 2002-0567).

Oocyte collection and *in vitro* maturation

Porcine ovaries were obtained from a local abattoir (Farm Story Dodarm B&F, Umsung, Chungbuk, Republic of Korea) and transported to the lab within 2 h of animal sacrifice in a thermos filled with physiological saline containing 50 mg/mL streptomycin sulfate and 75 mg/mL penicillin G at 30–37°C. Follicular fluid from follicles 3–6 mm in diameter was aspirated using a 12-gauge needle attached to a 10 mL disposable syringe. Cumulus-oocyte complexes (COCs) with uniform cytoplasm and three or more layers of cumulus granulosa cells were collected under a stereomicroscope for use in further experiments.

The *in vitro* maturation (IVM) medium used for oocyte maturation was ICM-199 (Invitrogen, USA) supplemented with 100 mg/L sodium pyruvate, 10 ng/mL epidermal growth factor, 10% (v/v) porcine follicular fluid, 10 IU/mL follicle-stimulating hormone (FSH), and 10 IU/mL luteinizing hormone (LH). After washing thrice with balanced IVM, approximately 80 COCs were transferred to each well of a 4-well plate (30004, SPL Life Sciences, Republic of Korea). The plate was then covered with mineral oil (370 μL/well) and incubated at 38.5°C for 42–44 h in an atmosphere of 5% CO_2 and 100% humidity.

Preparation of IDH2, GLUD1, and KMT5C dsRNA

IDH2, GLUD1, and KMT5C cDNA fragments were amplified from the total cDNA of porcine cumulus cells using primers containing the T7 promoter sequence (Supplementary Table S1). *In vitro* transcription was performed using a MEGAscript T7 Kit (AM1333; Thermo Fisher Scientific, USA), as described previously (Sun et al., 2023), to synthesize dsRNA following the manufacturer's instructions. After 10 h of *in vitro* transcription, the dsRNA mixture was treated with DNase I for 15 min to degrade the DNA template, then purified using Riboclear™ Plus (313-150, GeneAll Biotechnology, Republic of Korea). The purified dsRNA was dissolved in RNase-free water and stored at −80°C until use.

Parthenogenetic activation, dsRNA injection, and *in vitro* culture

After 44 h of IVM, COCs with extended cumulus cells were pipetted 20–30 times in a solution of 1 mg/mL hyaluronidase to remove cumulus cells. Oocytes at the MII stage, exhibiting the first polar body, were selected and parthenogenetically activated by two direct-current pulses of 120 V for 60 μs in 297 mmol/L mannitol (pH 7.2) containing 0.01% polyvinyl alcohol (PVA, w/v), 0.5 mmol/L HEPES, 0.05 mmol/L $MgSO_4$, and 0.1 mmol/L $CaCl_2$. The activated oocytes were then cultured in bicarbonate-buffered porcine zygote medium 5 (PZM-5) containing 7.5 μg/mL cytochalasin B and 5 mg/mL bovine serum albumin (BSA) for 3 h to suppress the extrusion of the pseudo-second polar body. After thorough washing, randomly and evenly grouped oocytes were microinjected with 5–10 pL of nucleus-free water or 1 200 ng/μL dsRNA using an Eppendorf Femto-Jet (Germany) under a Nikon Diaphot Eclipse TE300 inverted microscope (Japan). The oocytes were then transferred to *in vitro* culture (IVC) medium (bicarbonate-buffered PZM-5 supplemented with 5 mg/mL BSA) with increasing concentrations of dimethyl-α-KG (DM-α-KG; 0 μmol/L, 1 μmol/L, 5 μmol/L, 10 μmol/L, and 20 μmol/L) and cultured in a 5% CO_2 incubator at 38.5°C.

Immunofluorescence (IF) staining

In total, 10–15 embryos were collected and fixed in 3.7% formaldehyde for 1 h at room temperature (RT). After washing thrice in phosphate-buffered saline (PBS) containing 0.1% PVA (PBS-PVA) for 5 min, the embryos were permeabilized with 0.1% Triton X-100 for 30 min at RT. The embryos were again washed thrice and blocked with PBS/PVA containing 3% BSA for 1 h. Subsequently, the embryos were incubated with anti-IDH2 antibody (1:200, Abcam, ab131263, UK), GLUD1 polyclonal antibody (1:200, Proteintech, 14299-1-AP, China), anti-histone H4 (trimethyl K20) antibody (1:100,

Abcam, ab9053, UK), SIRT1 monoclonal antibody (1:100, Proteintech, 60303-1, China), caspase-3 rabbit mAb (1:200, Cell Signaling Technology, 9664S, USA), Ph2a.X antibody (1:100, Cell Signaling Technology, 2577S, USA), and Oct-3/4 antibody (1:100, Santa Cruz Biotechnology, USA) overnight at 4°C. After washing with PBS-PVA, the oocytes were cultured with Alexa Fluor 488™ donkey anti-mouse IgG (1:200, Invitrogen, A-21202, USA), Alexa Fluor 568™ donkey anti-mouse IgG (1:200, Invitrogen, A-11004, USA), Alexa Fluor 488™ donkey anti-rabbit IgG (1:200, Invitrogen, A-11034, USA), or Alexa Fluor 546™ donkey anti-rabbit IgG (1:200, Invitrogen, A-10040, USA) at 38.5°C for 1 h. After washing three times, the oocytes were mounted onto glass slides using an antifade mounting medium containing 4',6-diamidino-2-phenylindole (DAPI, VectorLabs, USA), and examined under a confocal microscope (LSM-880, Zeiss, Germany). Images were obtained using Zen software (v.3.10; Zeiss, Germany).

Mitochondrial distribution staining

Embryos were treated with 500 nmol/L MitoTracker Red CMXRos (M7512; Thermo Fisher Scientific, USA) in IVC medium at 38.5°C for 30 min. After washing thrice with PBS-PVA, the embryos were stained in a dark environment as described in the IF staining section.

EdU assay

A BeyoClick™ EdU Cell Proliferation Kit with Alexa Fluor 647 (Beyotime, China) was used for the cell proliferation assay. Briefly, morula (MO) stage embryos were incubated with 10 μmol/L EdU for 10 h at 38.5°C. The BLs were then fixed with 3.7% paraformaldehyde at RT for 30 min and permeabilized with 1% Triton X-100 for 30 min. After washing thrice with PBS/PVA, the BLs were incubated in 100 μL of click reaction cocktail in the dark for 30 min. After washing three times, the oocytes were mounted onto glass slides using an antifade mounting medium containing DAPI (VectorLabs, USA), and examined under a confocal microscope (LSM-880, Zeiss, Germany). Images were obtained using Zen software (v.3.10; Zeiss, Germany). The proliferation rate was calculated as the ratio of EdU-positive blastomeres to the total number of blastomeres.

Western blot analysis

One hundred embryos per group were sampled in 10 μL of RIPA buffer and 10 μL of loading buffer and heated at 95°C for 10 min. Whole proteins isolated from the oocytes were separated using 10% sodium dodecyl sulfate-polyacrylamide gel electrophoresis and electrically transferred onto polyvinylidene fluoride membranes. Subsequently, the membranes were blocked for 1 h with Tris-buffered saline with 0.1% Tween20 (TBST) containing 5% skim milk, then incubated overnight with recombinant anti-histone H3 (trimethyl K27) antibody (1:1 000, ab192985, Abcam, UK), anti-histone H3 (trimethyl K4) antibody (1:1 000, ab8580, Abcam, UK), anti-histone H3 (trimethyl K9) antibody (1:1 000, ab8898, Abcam, UK), GAPDH rabbit mAb (1:1 000, 5174S, Cell Signaling Technology, USA), and other indicated primary antibodies at 4°C. After washing thrice with TBST, the membranes were incubated with horseradish peroxidase (HRP)-conjugated goat anti-rabbit immunoglobulin G (IgG) or goat anti-mouse IgG (1:20 000; Santa Cruz Biotechnology, USA) antibodies at RT for 1 h, then finally exposed to SuperSignal West Femto Maximum Sensitivity Substrate (Thermo Fisher Scientific, USA). The membranes were imaged using a charge-coupled device camera and Nine Alliance Q9 software (v.18.00, Uvitec, Cambridge, UK). Band intensity was measured using ImageJ software (v2.0.0, National Institutes of Health, USA) for protein quantification, and relative band intensity was normalized to that of the housekeeping protein GAPDH.

RNA extraction, reverse transcription-quantitative real-time polymerase chain reaction (RT-qPCR)

RNA was extracted from 50 embryos per group using a Dynabead mRNA DIRECT kit (61012; Thermo Fisher Scientific, USA). cDNA was synthesized using a High-capacity cDNA Reverse Transcription Kit (4368814, Applied Biosystems, USA) according to the manufacturer's instructions. Reverse transcription was programmed as follows: 25°C for 10 min, 37°C for 120 min, and 85°C for 5 min. qPCR was performed using a Fast Real-Time PCR System (ABI StepOnePlus, Singapore). qPCR was performed using a WizPure qPCR Master Kit (W1731-8, Wizbiosolutions, Republic of Korea), with each reaction containing 10 μL of SYBR Green, 1 μL of each forward and reverse primer, and 1 μL of cDNA template adjusted to a final reaction volume of 20 μL. The amplification cycle was programmed as follows: 95°C for 3 min, followed by 40 cycles of 95°C for 15 s, 60°C for 25 s, 72°C for 10 s, and final extension at 72°C for 5 min. Biological and technical replicates were at least three times. The *GAPDH* gene was used as a reference gene. Primers were designed based on the CDS region of the target gene using Primer Premier (v.6.0) software. The primer sequences used in this study are listed in Supplementary Table S1. Relative gene expression was determined using the $2^{-\Delta\Delta CT}$ method.

A-KG assay

According to the manufacturer's protocols, 400 embryos/group were used to detect α-KG content using an Alpha Ketoglutarate (alpha KG) assay kit (ab83431; Abcam, UK).

Statistical analysis

All statistical analyses were performed using one-way analysis of variance (ANOVA) or Student's *t*-test with SPSS software (v.27.0.1.0; IBM SPSS, USA). All results are presented as mean±standard deviation (SD), with significance set to $P<0.05$. All experiments were repeated and performed at least three times. All schematics were drawn on the BioRender website (https://www.biorender.com/).

RESULTS

Subcellular distribution and expression of IDH2 and GLUD1 during porcine embryonic development

To investigate the expression and subcellular localization of IDH2 during embryonic development, we examined *IDH2* mRNA expression in 2C, 4-cell (4C), MO, and BL-stage embryos. *IDH2* mRNA expression increased from the 4C to BL stage compared to that at the 2C stage (Figure 1A). Subsequently, IF staining was performed to determine the subcellular location of IDH2. As shown in Figure 1B, C, the IDH2 protein was localized in the mitochondria, and its fluorescence intensity increased from the 4C stage, with the highest levels observed in the MO stage. In contrast, *GLUD1* mRNA expression increased from the 4C to MO stage and decreased in the BL stage, although was still higher than that in the 2C stage (Figure 1D). As shown in Figure 1E, F, the

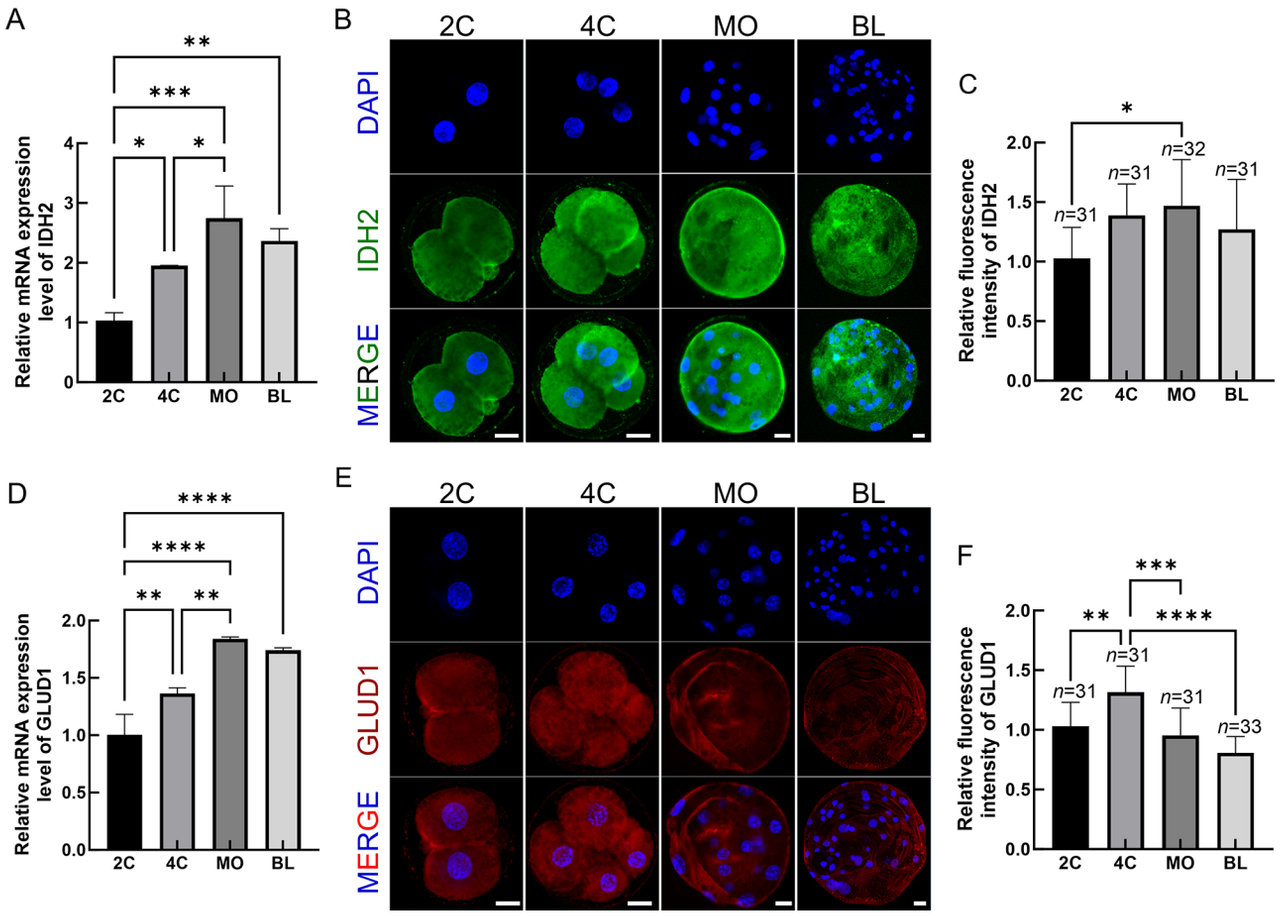

Figure 1 ***IDH2*** **and** ***GLUD1*** **mRNA and protein expression levels during early porcine embryonic development**

A: Relative expression of *IDH2* mRNA in 2-cell (2C), 4-cell (4C), morula (MO), and blastocyst (BL) stage embryos. B: Representative immunofluorescence (IF) images of IDH2 protein from 2C to BL stages. C: Relative fluorescence intensity of IDH2 protein. D: Relative expression of *GLUD1* mRNA from 2C to BL stages. E: Representative IF images of GLUD1 protein from 2C to BL stages. F: Relative fluorescence intensity of GLUD1 protein. Scale bar: 20 μm. ns: Not significant; *: $P<0.05$; **: $P<0.01$; ***: $P<0.001$; ****: $P<0.0001$.

GLUD1 protein was localized in the mitochondria, and its fluorescence intensity increased in the 4C stage and gradually decreased in the MO and BL stages.

IDH2 and GLUD1 KD results in intracellular α-KG depletion

To investigate the roles of IDH2 and GLUD1 in early porcine embryonic development, IDH2 and GLUD1 dsRNA (double gene KD, DKD) was microinjected into 1-cell (1C) stage embryos, which were then cultured in IVC medium. *GLUD1* mRNA expression at the 4C stage was assessed to verify KD efficiency (Figure 2A). Compared to the NC group (injected with water), *GLUD1* mRNA expression was significantly down-regulated after dsRNA microinjection. The IF results indicated that GLUD1 protein levels were also significantly reduced in DKD 4C stage embryos (Figure 2B, C). Similarly, *IDH2* mRNA expression was significantly down-regulated after dsRNA microinjection (Figure 2D), with IF showing that IDH2 protein levels were significantly lower in the DKD group than in the NC group (Figure 2E, F). DKD also led to defects in mitochondria (Figure 2E, F), the sites of oxidative phosphorylation (Kim et al., 2024). Reduced protein levels of IDH2 and GLUD1 following DKD were verified by western blotting, which showed that the protein levels of IDH2 and GLUD1 were significantly lower in the DKD group than in the NC group (Figure 2G, H). Changes in intracellular α-KG content at the 4C and BL stages were then detected, showing that α-KG content was significantly lower at the 4C and BL stages in the DKD group compared to the NC group (Figure 2I). These findings suggest that IDH2 and GLUD1 KD effectively interferes with the synthesis of intracellular α-KG, impairing the replenishment of consumed α-KG.

IDH2 and GLUD1 KD results in transcription repression in porcine embryos

The proliferation rates of 1C, 2C, 4C, 8C, MO, and BL stage embryos were next assessed at 0, 24, 48, 96, and 144 h, respectively. Results showed that the proportions of 4C and subsequent stage embryos were significantly lower in the DKD group than in the NC group, starting from 96 h (Figure 3A), suggesting that embryonic development was delayed at the EGA stage following IDH2 and GLUD1 KD. Hence, changes in the expression of EGA genes *DPPA2*, *WEE1*, *EIF1A*, *RIF1*, and *ZSCAN4* were detected in 4C embryos. As shown in Figure 3B, the expression levels of all tested EGA genes were down-regulated in the DKD group compared to the NC group.

The expression patterns of the early embryonic transcript product SIRT1 were further evaluated in 4C embryos (Zhang et al., 2022) (Figure 3C). Fluorescence intensity along the yellow line, traversing two nuclei, demonstrated that the SIRT1 protein was localized within the nucleus in the NC group, while nuclear localization was nearly absent in the DKD group. Consistent with these findings, the fluorescence intensity of SIRT1 was markedly lower in the DKD group compared to the

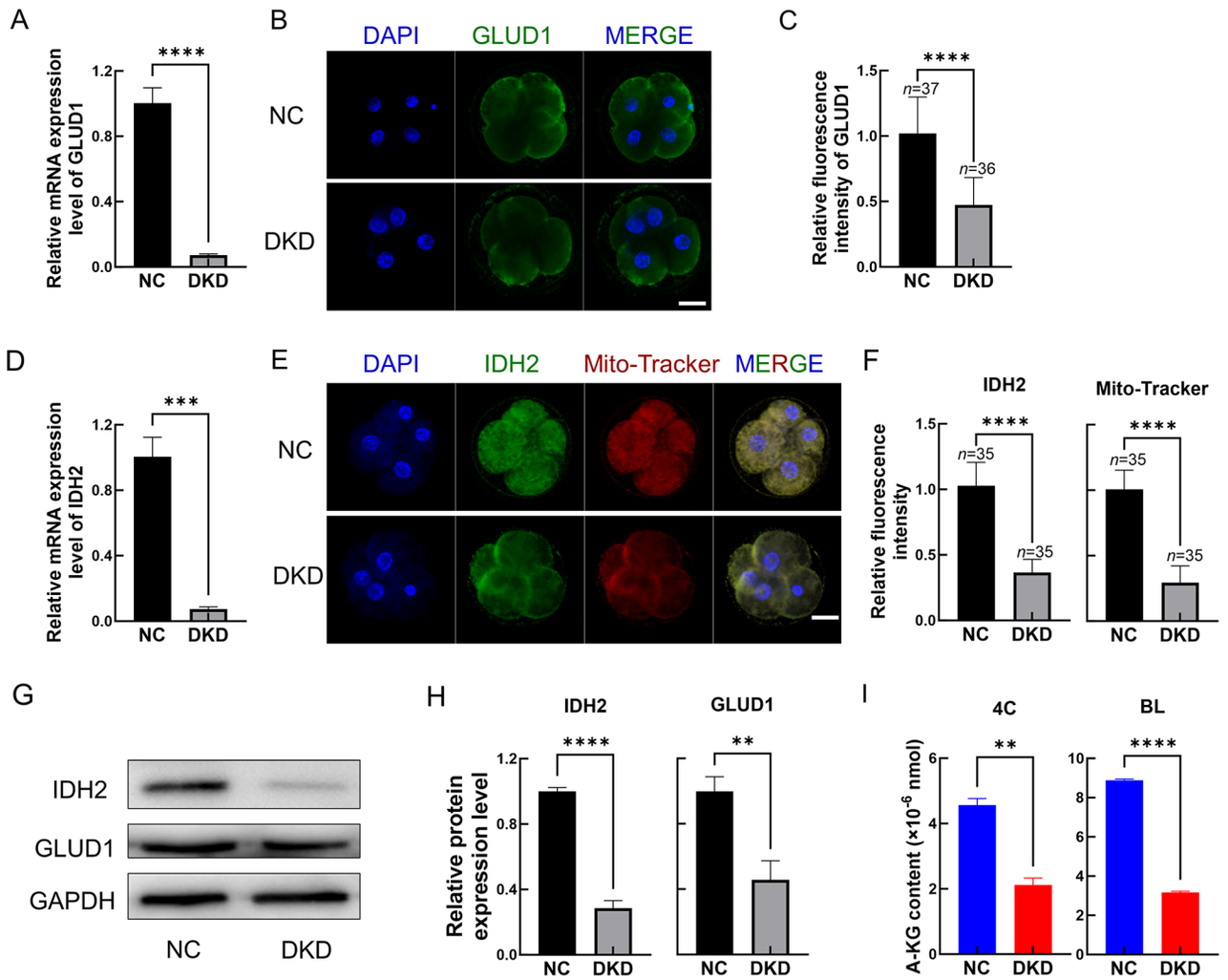

Figure 2 Effects of IDH2 and GLUD1 knockdown (KD) on intracellular α-ketoglutarate (α-KG) content

A: Relative expression of *GLUD1* mRNA in 4C stage embryos following injection of IDH2 and GLUD1 dsRNA mix (DKD). Nuclear-free water was injected into porcine parthenotes as the control group (NC). B: Representative immunofluorescence (IF) staining images of GLUD1 protein. C: Relative fluorescence intensity of GLUD1 protein. D: Relative expression of *IDH2* mRNA in NC and DKD 4C stage embryos. E: Representative IF images of IDH2 protein and Mito-Tracker Red CMXRos. F: Relative fluorescence intensity of IDH2 protein and Mito-Tracker Red CMXRos. G: Representative western blot images of IDH2 and GLUD1; GAPDH was used as the internal reference protein. H: Relative protein levels of IDH2 and GLUD1 in NC and DKD 4C stage embryos. I: Changes in intracellular α-ketoglutarate (α-KG) content in NC and DKD 4C and BL stage embryos. Scale bar: 20 μm. ns: Not significant; *: P<0.05; **: P<0.01; ***: P<0.001; ****: P<0.0001.

NC group (Figure 3D). Collectively, these results suggest that IDH2 and GLUD1 KD significantly impairs and delays porcine embryonic development and induces transcriptional repression of the EGA genes.

IDH2 and GLUD1 KD impairs BL quality

The impact of IDH2 and GLUD1 KD on BLs was assessed, revealing a significant reduction in BL formation in the DKD group compared to the NC group (Figure 4A). DNA damage in porcine BLs was evaluated by examining γH2Ax levels (Figure 4B, C), which were notably higher in the DKD group compared to the NC group, indicating increased DNA damage. Hence, the effects of DKD on apoptosis and proliferation were analyzed using IF for caspase-3 (CASP3) and EdU staining (Figure 4D). Results showed that apoptosis was significantly increased in the DKD group compared to the NC group, as indicated by increased CASP3 levels (Figure 4E), while blastomere proliferation was markedly decreased (Figure 4F).

OCT4, a marker of ICM and cell pluripotency (Lee et al., 2022), showed a significant decrease in the ratio of OCT4 positive (OCT4$^+$) cells to total nuclei in the DKD group relative to the NC group (Figure 4G, H). Additionally, the diameter and total cell count of BLs were significantly lower in the DKD group compared to the NC group (Figure 4I, J). Collectively, these findings suggest that IDH2 and GLUD1 KD induces embryonic DNA damage and apoptosis, impairs BL lineage differentiation, and reduces pluripotency.

DM-α-KG supplementation restores normal H4K20me3 levels in 4C stage

To verify that reduced intracellular α-KG levels, resulting from IDH2 and GLUD1 KD, were the primary cause of EGA failure and compromised BL quality, cell membrane-permeable DM-αKG (0, 1, 5, 10, and 20 μmol/L) was introduced into the culture medium during *in vitro* embryo culture after IDH2 and GLUD1 KD. Evaluation of embryonic development demonstrated that DM-α-KG supplementation effectively improved the development rate in the DKD group (Figure 5A). A concentration of 10 μmol/L DM-α-KG was selected for

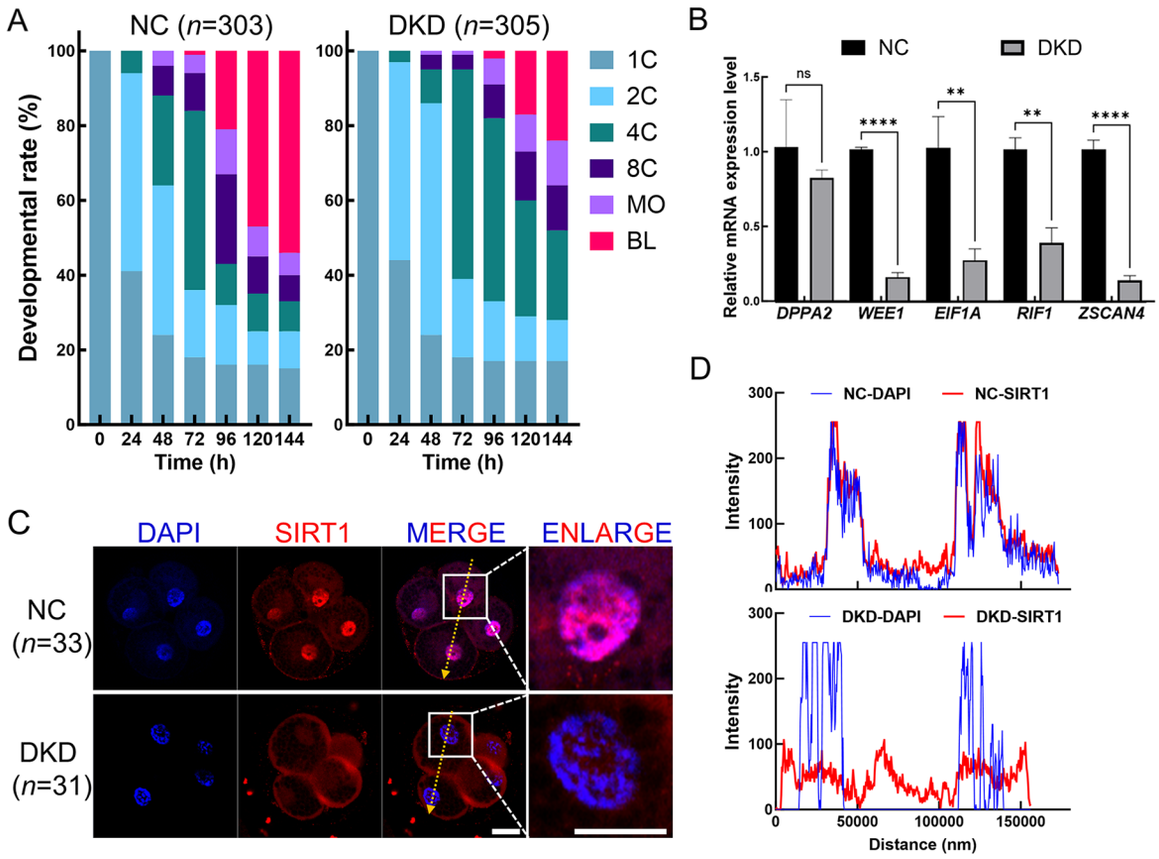

Figure 3 Effects of IDH2 and GLUD1 knockdown (KD) on porcine EGA

A: Proportion of 1-cell (1C), 2C, 4C, 8-cell (8C), MO, and BL stage embryos to all embryos at 0, 24, 48, 72, 96, 120, and 144 h post-KD. B: Relative mRNA expression of embryonic genome activation (EGA)-related genes (*DPPA2*, *WEE1*, *EIF1A*, *RIF1*, and *ZSCAN4*) in NC and DKD 4C stage embryos. C: Representative IF images of early transcription product SIRT1 in NC and DKD 4C stage embryos. Scale bars: 20 μm. D: Changes in fluorescence intensity at yellow line of SIRT1 protein and DAPI. ns: Not significant; *: $P<0.05$; **: $P<0.01$; ***: $P<0.001$; ****: $P<0.0001$.

further experiments. Subsequently, several histone modifications associated with transcriptional repression were detected. Results showed that IDH2 and GLUD1 KD led to increased expression of H4K20me3, H3K9me3, and H3K4me3, and decreased expression of H3K27me3. Notably, the addition of DM-α-KG reversed the increases in H4K20me3 and H3K9me3. Among the histone modifications examined, H4K20me3 was the most significantly affected by IDH2 and GLUD1 KD and DM-α-KG supplementation (Figure 5B, C). IF analysis confirmed these observations, showing that H4K20me3 fluorescence intensity was significantly reduced in 4C stage embryos following DM-α-KG supplementation compared to the DKD group (Figure 5D, E). Collectively, these findings suggest that abnormally high expression of H4K20me3 may be the main cause of transcriptional repression induced by IDH2 and GLUD1.

IDH2 and GLUD1 KD disrupts H4K20me3 reprogramming

IDH2 and GLUD1 KD can lead to the depletion of intracellular α-KG, a critical cofactor for α-KG-dependent dioxygenases, including the H4K20me3 demethylase RAD23 (Figure 6A). To determine whether this depletion affects H4K20me3 levels in porcine embryos, we investigated the expression of H4K20me3 at various stages of early embryonic development. Results showed that H4K20me3 levels decreased from the 4C stage onward, with a subsequent increase at the BL stage; however, levels remained lower than those observed at the 1C and 2C stages (Figure 6B, C). The IF results showed similar changes in H4K20me3 levels at various stages of embryonic development and after DKD in 4C stage embryos (Figure 6D). H4K20me3 levels decreased from the 4C stage and increased from the MO stage, although levels were still lower than those observed at the 1C and 2C stages. In contrast, embryos in the DKD group exhibited persistently high H4K20me3 levels, which did not decrease at the 4C stage and remained elevated through the BL stage, exceeding levels in the NC group (Figure 6E).

KMT5C KD enhances developmental potential

To further determine whether H4K20me3 acts as an epigenetic barrier in porcine embryonic development, particularly under IDH2 and GLUD1 KD, we knocked down the H4K20me3 methyltransferase KMT5C. As shown in Figure 7A, injection of KMT5C dsRNA significantly reduced the expression levels of KMT5C mRNA. Western blot analysis further confirmed that KMT5C KD significantly reduced the expression of H4K20me3 in DKD embryos (Figure 7B, C). Interestingly, KMT5C KD also resulted in a marked improvement in the BL formation rate in porcine PA embryos. Additionally, a synergistic effect was observed with the addition of DM-α-KG, further enhancing BL formation (Figure 7D).

DM-α-KG supplementation and KMT5C KD improve porcine BL quality

Given that both DM-α-KG supplementation and KMT5C KD

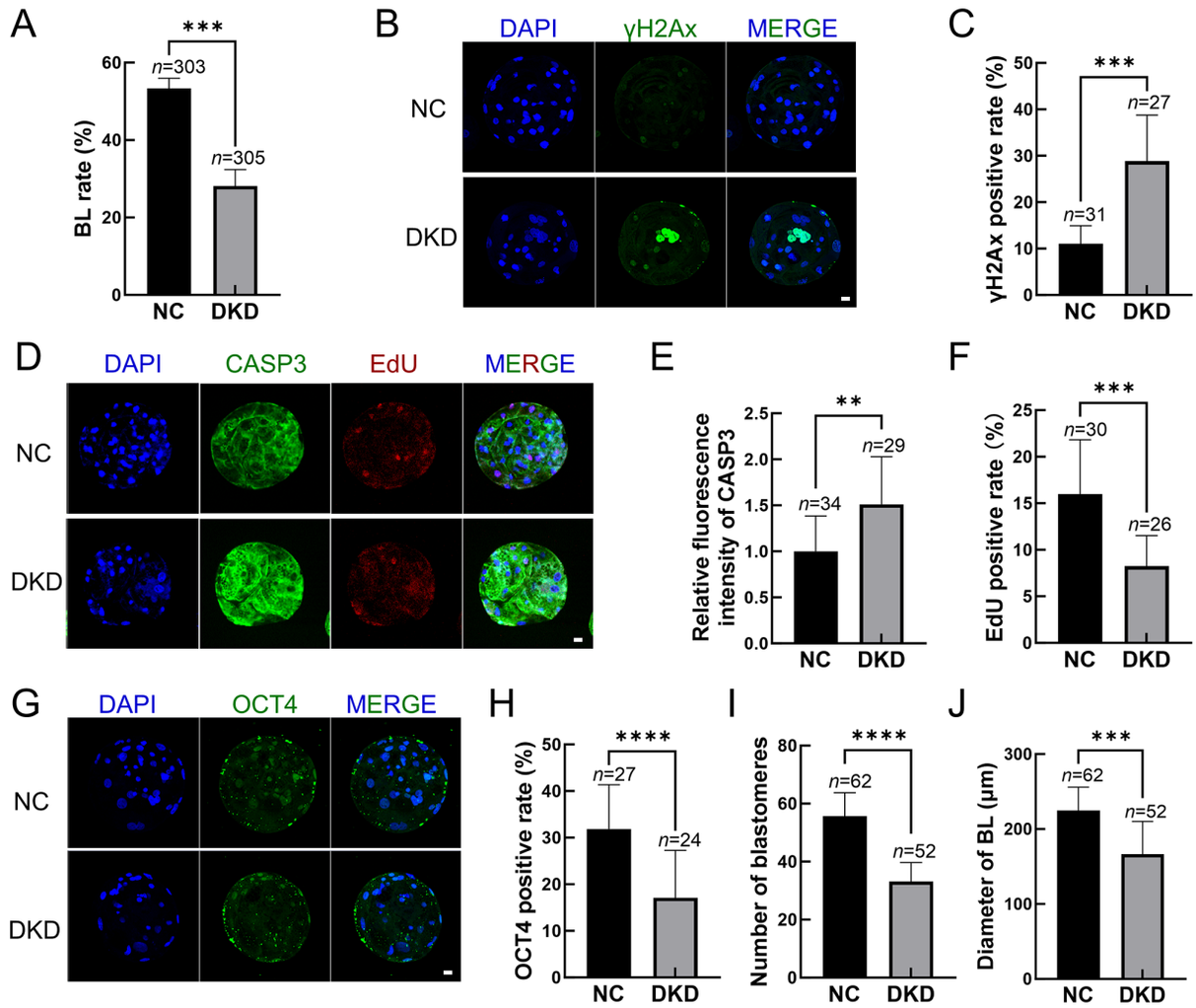

Figure 4 Effects of IDH2 and GLUD1 knockdown (KD) on porcine BL quality

A: BL rate in NC and DKD groups. B: Representative IF images of γH2Ax in NC and DKD BLs. C: Ratio of γH2Ax positive/total nuclei in NC and DKD BLs. D: Representative IF images of caspase-3 (CASP3) protein and EdU staining in NC and DKD BLs. E: Relative fluorescence intensity of CASP3 protein in NC and DKD BLs. F: Ratio of EdU positive/total nuclei in NC and DKD BLs. G: Representative IF images of OCT4 protein in NC and DKD BLs. H: Ratio of OCT4 positive/total nuclei in NC and DKD BLs. I: Total blastomere number in NC and DKD groups. J: BL diameter in NC and DKD groups. Scale bar: 20 μm. ns: Not significant; *: P<0.05; **: P<0.01; ***: P<0.001; ****: P<0.0001.

can normalize H4K20me3 levels and significantly increase BL formation rates, we speculated that these interventions could also improve BL quality in the context of IDH2 and GLUD1 KD. To assess this, DNA damage was evaluated by measuring γH2Ax levels in BLs (Figure 8A). Results showed that DNA damage was markedly reduced in the DKD+α-KG, DKD+KMT5C KD, and DKD+α-KG+KMT5C KD groups compared to the DKD group, with the DKD+α-KG+KMT5C KD group showing the lowest level of DNA damage (Figure 8B). Apoptosis and proliferation were evaluated using IF for CASP3 and EdU staining, respectively (Figure 8C). Results showed that apoptosis levels decreased significantly in the DKD+α-KG, DKD+KMT5C KD, and DKD+α-KG+KMT5C KD groups compared to the DKD group (Figure 8D). Furthermore, blastomere proliferation was significantly increased in the DKD+α-KG, DKD+KMT5C KD, and DKD+α-KG+KMT5C KD groups compared to the DKD group (Figure 8E). The ratio of $OCT4^+$ cells to total nuclei was higher in the DKD+α-KG, DKD+KMT5C KD, and DKD+α-KG+KMT5C KD groups than in the DKD group (Figure 8F, G. Collectively, these results indicate that DM-α-KG supplementation and KMT5C KD can reverse IDH2 and GLUD1 KD-induced DNA damage and apoptosis in BLs, promote blastomere proliferation, and increase pluripotency.

DISCUSSION

Mammalian preimplantation embryonic development involves extensive epigenetic reprogramming to facilitate the transition from maternal epigenetic control to zygotic genome activation. Recent studies have highlighted the role of various metabolites in regulating this complex process. However, the specific contributions of IDH2 and GLUD1 to epigenetic modifications during early porcine embryogenesis remain poorly understood. In the present study, we investigated the role of α-KG in porcine embryo development through targeted IDH2 and GLUD1 KD.

IDH2 is the rate-limiting enzyme in the TCA cycle, catalyzing the production of α-KG from isocitrate (Al-Khallaf, 2017). In contrast, GLUD1, an important enzyme in glutaminolysis, produces α-KG through its glutamate dehydrogenation activity (Nagao et al., 2017). Both enzymes are integral to maintaining intracellular α-KG levels, which are essential for various biological processes, including epigenetic

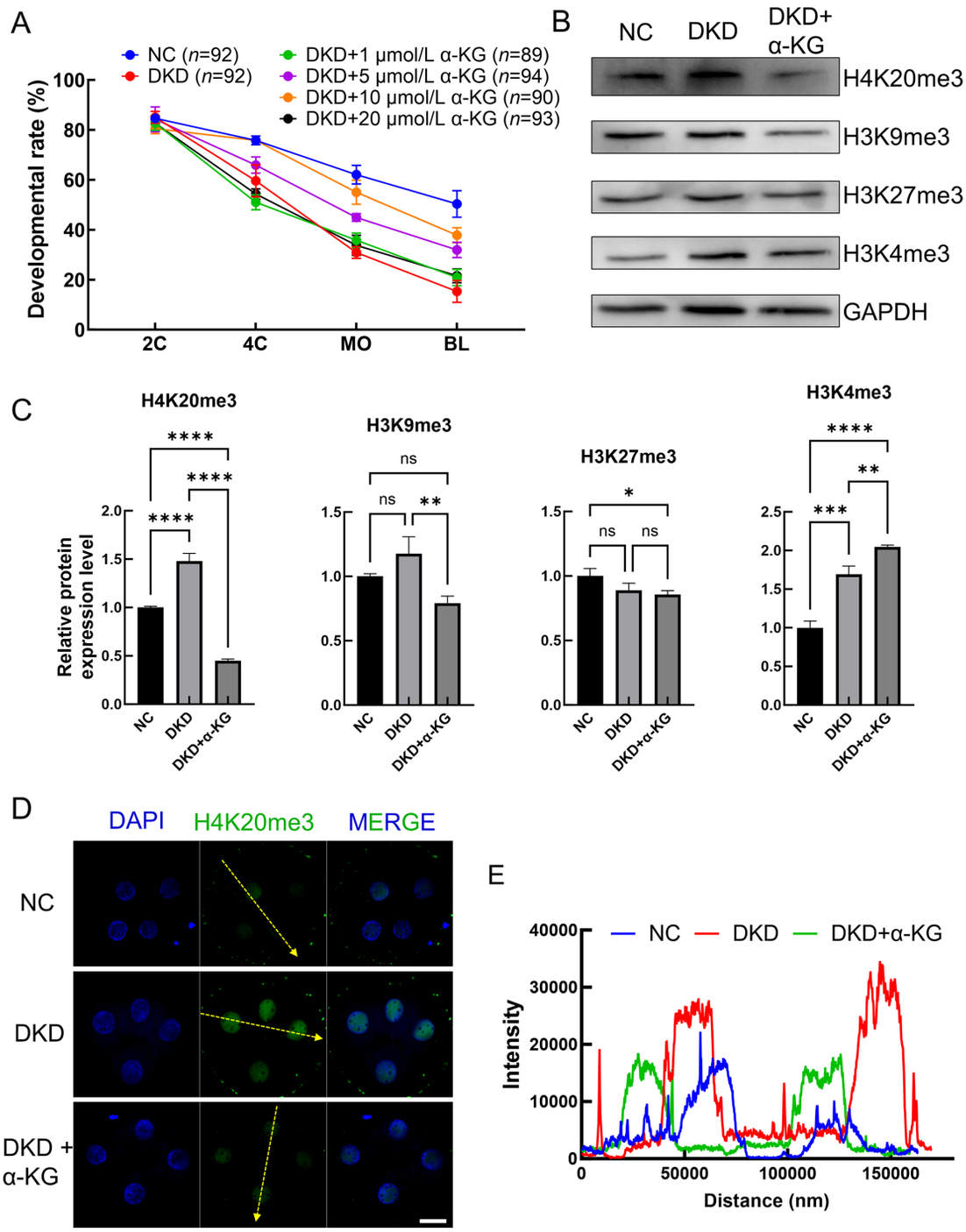

Figure 5 Effects of IDH2 and GLUD1 knockdown (KD) and dimethyl-α-KG (DM-α-KG) supplementation on histone modifications in porcine embryos

A: Embryonic developmental rates in NC, DKD, DKD+1 μmol/L DM-α-KG, DKD+5 μmol/L DM-α-KG, DKD+10 μmol/L DM-α-KG, and DKD+20 μmol/L DM-α-KG groups. B: Representative western blot images in 4C stage embryos of NC, DKD, and DKD+10 μmol/L DM-α-KG (DKD+α-KG) groups; GAPDH was used as the internal reference protein. C: Relative protein levels in 4C stage embryos of NC, DKD, and DKD+α-KG groups. D: Representative IF images of H4K20me3 in 4C stage embryos of NC, DKD, and DKD+α-KG groups. Scale bar: 20 μm. E: Fluorescence intensity of H4K20me3 at yellow line in 4C stage embryos of NC, DKD, DKD+α-KG groups. ns: Not significant; *: $P<0.05$; **: $P<0.01$; ***: $P<0.001$; ****: $P<0.0001$.

regulation. In embryonic stem cells, chaperone-mediated autophagy degrades IDH1 and IDH2 and reduces intracellular α-KG levels, thereby decreasing stem cell pluripotency (Xu et al., 2020). Similarly, a significant reduction in intracellular α-KG levels has been reported in kidney renal clear cell carcinoma cells following GLUD1 depletion (Shao et al., 2021). Furthermore, GLUD1 has been identified as a potential DNA marker linked to enhanced reproductive traits in Jining Grey goats (Wang et al., 2023), highlighting its vital role in mammalian reproduction.

In this study, IDH2 and GLUD1 exhibited elevated mRNA and protein expression at the 4C stage, suggesting that this period may represent a critical window for their functional activity during early porcine embryonic development. This increased expression appears to coincide with the growing demand for α-KG as the embryo transitions from a

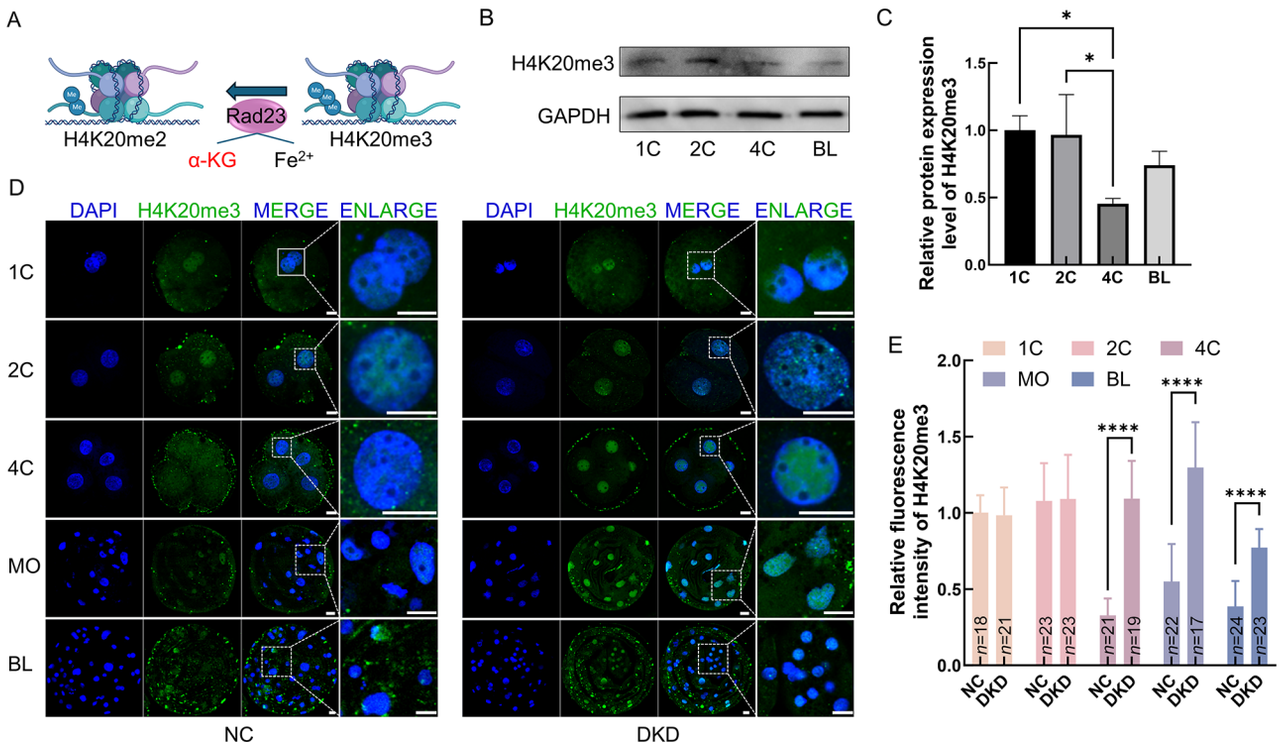

Figure 6 Effects of IDH2 and GLUD1 knockdown (KD) on H4K20me3 levels in porcine embryos

A: α-KG is a cofactor of H4K20me3 demethylase RAD23. B: Representative western blot images of H4K20me3 in 1C, 2C, 4C, and BL stage embryos; GAPDH was used as the internal reference protein. C: Relative H4K20me3 protein levels in 1C, 2C, 4C, and BL stage embryos. D: Representative IF images of H4K20me3 in NC and DKD 1C, 2C, 4C, MO, and BL stage embryos. Scale bars: 20 μm. E: Relative fluorescence intensity of H4K20me3 in NC and DKD 1C, 2C, 4C, MO, and BL stage embryos. ns: Not significant; *: P<0.05; **: P<0.01; ***: P<0.001; ****: P<0.0001.

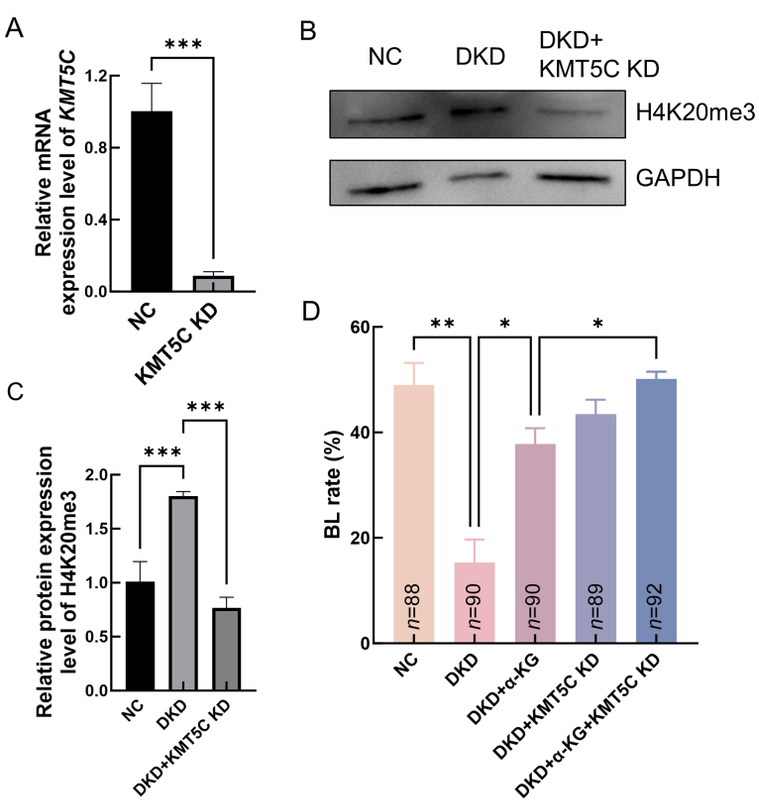

Figure 7 Effects of KMT5C knockdown (KD) and DM-α-KG supplementation on porcine embryonic development ability

A: Relative expression of KMT5C mRNA in NC and KMT5C KD embryos. B: Representative western blot images of H4K20me3 protein in NC, DKD, and DKD+KMT5C KD embryos at 4C stage. C: Relative H4K20me3 protein levels in NC, DKD, and DKD+KMT5C KD embryos at 4C stage. D: BL formation rate in NC, DKD, DKD+α-KG, DKD+KMT5C KD, and DKD+α-KG+KMT5C KD groups. ns: Not significant; *: P<0.05; **: P<0.01; ***: P<0.001; ****: P<0.0001.

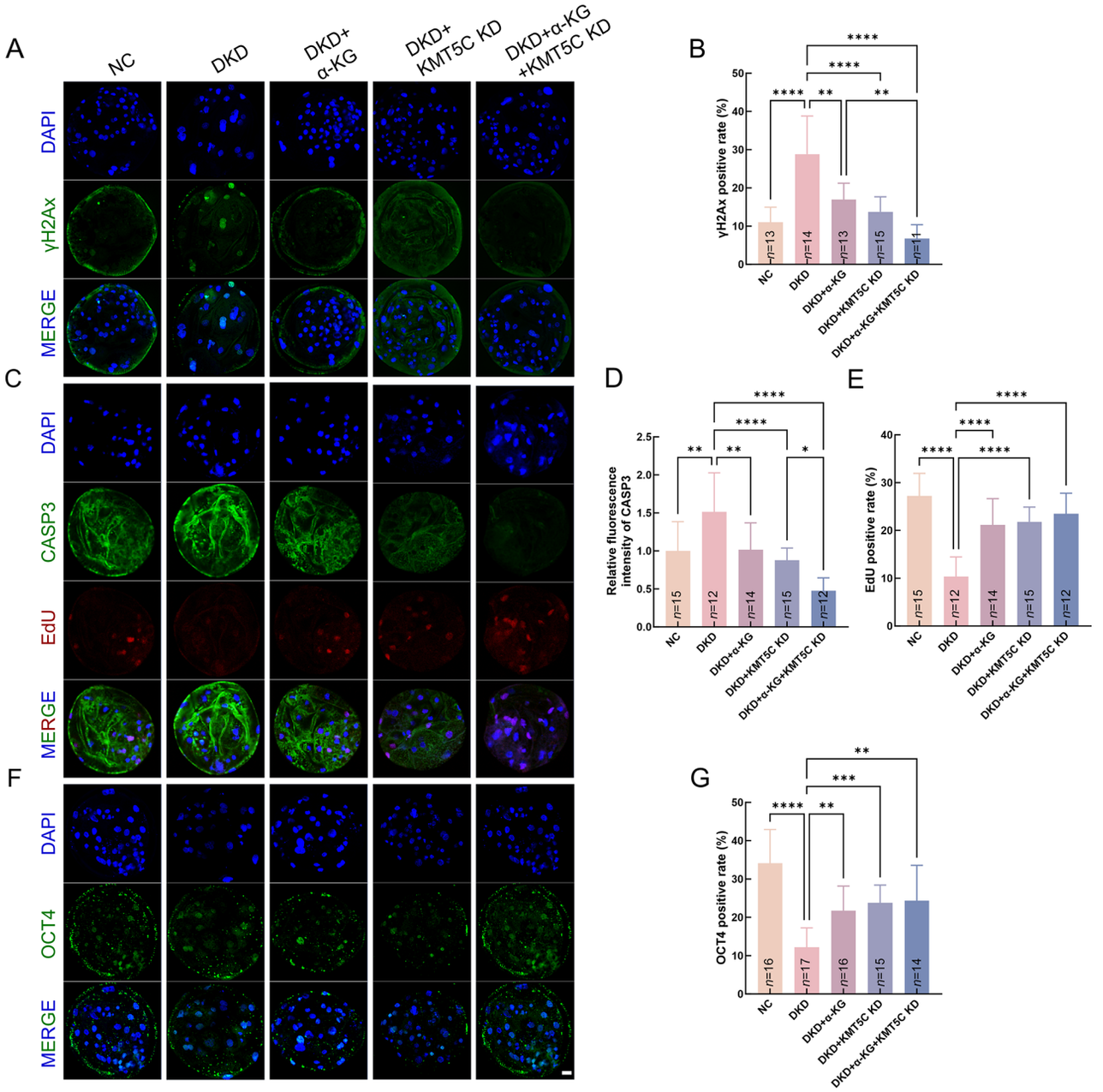

Figure 8 Effects of KMT5C knockdown (KD) and DM-α-KG supplementation on porcine blastocyst (BL) quality

A: Representative IF images of γH2Ax in NC, DKD, DKD+α-KG, DKD+KMT5C KD, and DKD+α-KG+KMT5C KD BLs. B: Ratio of γH2Ax positive/total nuclei in NC, DKD, DKD+α-KG, DKD+KMT5C KD, and DKD+α-KG+KMT5C KD BLs. C: Representative IF images of CASP3 protein and EdU staining in NC, DKD, DKD+α-KG, DKD+KMT5C KD, and DKD+α-KG+KMT5C KD BLs. D: Relative fluorescence intensity of CASP3 protein in NC, DKD, DKD+α-KG, DKD+KMT5C KD, and DKD+α-KG+KMT5C KD BLs. CASP3: Caspase-3. E: Ratio of EdU positive/total nuclei in NC, DKD, DKD+α-KG, DKD+KMT5C KD, and DKD+α-KG+KMT5C KD BLs. F: Representative IF images of OCT4 protein in NC, DKD, DKD+α-KG, DKD+KMT5C KD, and DKD+α-KG+KMT5C KD BLs. G: Ratio of OCT4 positive/total nuclei in NC, DKD, DKD+α-KG, DKD+KMT5C KD, and DKD+α-KG+KMT5C KD BLs. Scale bar: 20 μm. ns: Not significant; *: P<0.05; **: P<0.01; ***: P<0.001; ****: P<0.0001.

metabolically quiescent state at ovulation to a highly active metabolic state at implantation. During this transition, key metabolic processes are activated, including the methionine cycle from the 8-cell stage to the BL, heightened glutaminolysis in the BL, enhanced TCA cycle activity from the 8-cell embryo stage, and increased glycolysis in the BL (Li et al., 2022). Many pathways, such as amino acid biosynthesis and fatty acid metabolism, are active at the 4C stage (i.e., EGA stage), but not at the 2C and zygote stages (Xiang et al., 2020), indicating that these metabolic pathways and their resultant metabolites are critical for EGA. In embryos subjected to IDH2 and GLUD1 KD, a notable reduction in mitochondrial signaling was observed, suggesting that IDH2 and GLUD1 KD impairs mitochondrial function, thereby affecting metabolism.

In this study, intracellular α-KG content was significantly depleted following IDH2 and GLUD1 KD, resulting in disrupted porcine embryonic development. Proper early embryonic development requires the correct reprogramming and configuration of gene networks by the timely and faithful execution of EGA. Impaired EGA is a key factor underlying early embryonic developmental arrest in mammals (Chen

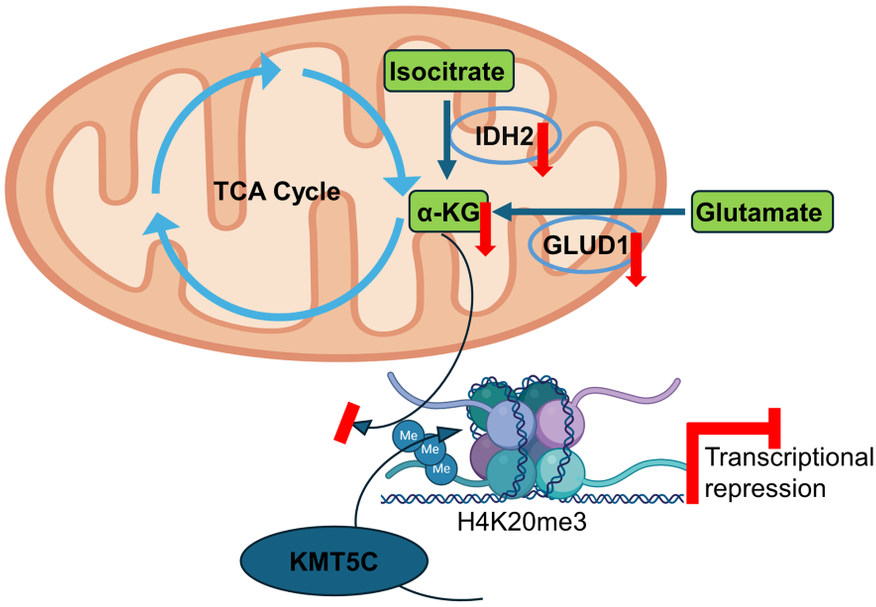

Figure 9 Schematic of effects of IDH2 and GLUD1 knockdown (KD) on porcine embryonic development

The IDH2 and GLUD1 enzymes produce intracellular α-KG. Hence, IDH2 and GLUD1 KD results in depletion of intracellular α-KG content, which impairs H4K20me3 demethylation. Thus, intracellular α-KG depletion impairs embryonic development through transcriptional repression as a result of high H4K20me3 levels.

et al., 2016; Sfakianoudis et al., 2021). The most obvious manifestation of EGA is a dramatic increase in transcriptional activity (Kong et al., 2020). In this study, the expression of critical EGA-related genes, including *DPPA2*, *WEE1*, *EIF1A*, *RIF1*, and *ZSCAN4*, was significantly down-regulated in DKD embryos at the 4C stage. SIRT1, a known early transcriptional marker in mouse and porcine embryos, plays a vital role in EGA (Nagaraj et al., 2017; Zhou et al., 2020). Elevated SIRT1 expression in porcine zygotes has been shown to promote BL formation (Adamkova et al., 2017). In the present study, however, SIRT1 protein expression was markedly decreased in the DKD group, further suggesting impairment of EGA following α-KG depletion.

Concurrent with the decrease in embryonic developmental capacity, BL quality was significantly diminished in the DKD group. Higher levels of DNA damage and apoptosis, coupled with lower proliferative capacity, were evident in DKD-derived BLs. Additionally, the proportion of $OCT4^+$ cells in DKD BLs was significantly decreased, indicating a notable reduction in embryonic pluripotency due to α-KG depletion. These observations align with previous studies showing that α-KG plays a pivotal role in maintaining naïve pluripotency and promoting the transient potential for primordial germ cell fate by regulating the balance between H3K9me2 acquisition and H3K27me3 depletion (Tischler et al., 2019). Consequently, our findings further confirm the important role of α-KG in the regulation of histone modifications.

α-KG is essential for protein and DNA demethylation and promotes major genomic reprogramming (Martinez-Pastor et al., 2013). As a cofactor for demethylases, including RAD23, a demethylase of H4K20me3 (Cao et al., 2020), α-KG regulates various histone modifications (Kaelin & McKnight, 2013; Zhang et al., 2019). Here, we observed a decrease in H4K20me3 levels starting from the 4C stage, consistent with its function in gene silencing (Magaraki et al., 2017), as a large number of genes need to be transcribed during EGA. However, the DKD group exhibited abnormally high levels of H4K20me3, which likely contributed to EGA failure and embryonic growth arrest due to α-KG depletion during early porcine embryonic development. These findings are consistent with previous studies demonstrating unusually high H4K20me3 levels in mouse SCNT embryos, where aberrant H4K20me3 levels functioned as an epigenetic barrier to NT reprogramming and Suv4-20h2 KD markedly enhanced BL formation in NT mouse embryos (Liu et al., 2024).

Previous studies have reported that supplementation with membrane-permeable DM-αKG enhances stem cell pluripotency (Carey et al., 2015; Hwang et al., 2016; Xu et al., 2020) and supports the *in vitro* development of BLs from mouse zygotes cultured in pyruvate-deficient medium (Choi et al., 2019). Additionally, targeting specific histone modification enzymes has been shown to improve SCNT reprogramming efficiency. For example, induction of Kds4d, a demethylase of H3K9me3, in embryonic stem cells has been shown to decrease H3K9me3 levels and improve *in vitro* development in cloned embryos (Antony et al., 2013). Kdm4d can also reactivate most reprogramming-resistant regions, significantly improving SCNT efficiency (Matoba et al., 2014). Similarly, overexpression of KDM6A in bovine SCNT embryos can effectively reduce the H3K27me3 barrier and enhance embryo developmental capacity (Zhou et al., 2019). Therefore, in the present study, we knocked down KMT5C and supplemented DM-α-KG in the IVC medium after IDH2 and GLUD1 KD. This dual intervention effectively improved the developmental capacity of porcine embryos and reduced H4K20me3 levels, reversing the effects of IDH2 and GLUD1 KD. Additionally, KMT5C KD and DM-α-KG supplementation decreased DNA damage and apoptosis levels in DKD porcine BLs and increased the proliferative ability of DKD BLs. The proportion of $OCT4^+$ cells, indicative of pluripotency, also increased in response to these treatments. Furthermore, KMT5C KD, combined with DM-α-KG, had a synergistic effect on the developmental rate and BL quality of porcine PA embryos.

This study has several limitations. First, we did not comprehensively explore the effects of IDH2 and GLUD1 KD on the overall metabolic state of porcine embryos. Second, we did not investigate the effects of knocking down or overexpressing other histone methyltransferases. Future research should focus on elucidating the precise mechanisms by which α-KG modulates histone modifications and investigating potential interventions to regulate α-KG levels. Such approaches could enhance embryonic development and overcome epigenetic barriers.

In conclusion, our study demonstrated that IDH2 and GLUD1 are highly expressed at the 4C stage in porcine embryos, and knockdown of these enzymes leads to significant depletion of intracellular α-KG. This depletion results in elevated levels of H4K20me3, a gene-silencing histone modification, which must be withdrawn during EGA for normal embryonic development. The persistence of high H4K20me3 levels following intracellular α-KG depletion acts as an epigenetic barrier during the EGA period, leading to transcriptional repression and developmental arrest (Figure 9). Overall, this study highlights the critical role of IDH2 and GLUD1 in regulating H4K20me3 reprogramming during early embryogenesis, establishing a link between IDH2, GLUD1, and epigenetic modifications during early porcine embryonic development, and shedding light on the involvement of energy metabolism in epigenetic regulation at large.

SUPPLEMENTARY DATA

Supplementary data to this article can be found online.

COMPETING INTERESTS

The authors declare that they have no competing interests.

AUTHORS' CONTRIBUTIONS

X.S.C. and C.L.Z. designed the experiment. C.L.Z. drafted the manuscript. X.S.C. reviewed and edited the manuscript. C.L.Z. and Q.Y.L. completed the main experiments. S.H.L., X.H.L., and J.D.K. participated in the collection of samples and methodology. G.H.L., J.M.S., H.J.S., and Y.Y.J. participated in data analysis and visualization. All authors read and approved the final version of the manuscript.

REFERENCES

Adamkova K, Yi YJ, Petr J, et al. 2017. SIRT1-dependent modulation of methylation and acetylation of histone H3 on lysine 9 (H3K9) in the zygotic pronuclei improves porcine embryo development. *Journal of Animal Science and Biotechnology*, **8**: 83.

Al-Khallaf H. 2017. Isocitrate dehydrogenases in physiology and cancer: biochemical and molecular insight. *Cell & Bioscience*, **7**: 37.

Antony J, Oback F, Chamley LW, et al. 2013. Transient JMJD2B-mediated reduction of H3K9me3 levels improves reprogramming of embryonic stem cells into cloned embryos. *Molecular and Cellular Biology*, **33**(5): 974–983.

Balakrishnan L, Milavetz B. 2010. Decoding the histone H4 lysine 20 methylation mark. *Critical Reviews in Biochemistry and Molecular Biology*, **45**(5): 440–452.

Cao XW, Chen YR, Wu B, et al. 2020. Histone H4K20 demethylation by two hHR23 proteins. *Cell Reports*, **30**(12): 4152–4164. e6.

Carey BW, Finley LWS, Cross JR, et al. 2015. Intracellular α-ketoglutarate maintains the pluripotency of embryonic stem cells. *Nature*, **518**(7539): 413–416.

Chen JM, Lian XL, Du J, et al. 2016. Inhibition of phosphorylated Ser473-Akt from translocating into the nucleus contributes to 2-cell arrest and defective zygotic genome activation in mouse preimplantation embryogenesis. *Development, Growth & Differentiation*, **58**(3): 280–292.

Choi ES, Kawano K, Hiraya M, et al. 2019. Effects of pyruvate and dimethyl-α-ketoglutarate, either alone or in combination, on pre- and post-implantation development of mouse zygotes cultured in vitro. *Reproductive Medicine and Biology*, **18**(4): 405–410.

Figueroa ME, Abdel-Wahab O, Lu C, et al. 2010. Leukemic IDH1 and IDH2 mutations result in a hypermethylation phenotype, disrupt TET2 function, and impair hematopoietic differentiation. *Cancer Cell*, **18**(6): 553–567.

Hwang IY, Kwak S, Lee S, et al. 2016. Psat1-dependent fluctuations in α-ketoglutarate affect the timing of ESC differentiation. *Cell Metabolism*, **24**(3): 494–501.

Jørgensen S, Schotta G, Sørensen CS. 2013. Histone H4 lysine 20 methylation: key player in epigenetic regulation of genomic integrity. *Nucleic Acids Research*, **41**(5): 2797–2806.

Kaelin WG Jr, McKnight SL. 2013. Influence of metabolism on epigenetics and disease. *Cell*, **153**(1): 56–69.

Kim MJ, Jeon SB, Kang HG, et al. 2024. Cadmium exposure impairs porcine embryonic development by inducing oxidative stress and mitochondrial dysfunction. *Journal of Animal Reproduction and Biotechnology*, **39**(1): 48–57.

Kong QR, Yang X, Zhang H, et al. 2020. Lineage specification and pluripotency revealed by transcriptome analysis from oocyte to blastocyst in pig. *The FASEB Journal*, **34**(1): 691–705.

Lee M, Oh JN, Choe GC, et al. 2022. Changes in OCT4 expression play a crucial role in the lineage specification and proliferation of preimplantation porcine blastocysts. *Cell Proliferation*, **55**(11): e13313.

Li JY, Zhang JM, Hou WB, et al. 2022. Metabolic control of histone acetylation for precise and timely regulation of minor ZGA in early mammalian embryos. *Cell Discovery*, **8**(1): 96.

Liu WQ, Liu XY, Wang CF, et al. 2016. Identification of key factors conquering developmental arrest of somatic cell cloned embryos by combining embryo biopsy and single-cell sequencing. *Cell Discovery*, **2**: 16010.

Liu ZH, Wang WG, Xia YH, et al. 2024. Overcoming the H4K20me3 epigenetic barrier improves somatic cell nuclear transfer reprogramming efficiency in mice. *Cell Proliferation*, **57**(1): e13519.

Magaraki A, Van Der Heijden G, Sleddens-Linkels E, et al. 2017. Silencing markers are retained on pericentric heterochromatin during murine primordial germ cell development. *Epigenetics & Chromatin*, **10**: 11.

Martinez-Pastor B, Cosentino C, Mostoslavsky R. 2013. A tale of metabolites: the cross-talk between chromatin and energy metabolism. *Cancer Discovery*, **3**(5): 497–501.

Matoba S, Liu YT, Lu FL, et al. 2014. Embryonic development following somatic cell nuclear transfer impeded by persisting histone methylation. *Cell*, **159**(4): 884–895.

Nagao H, Nishizawa H, Bamba T, et al. 2017. Increased dynamics of tricarboxylic acid cycle and glutamate synthesis in obese adipose tissue: in vivo metabolic turnover analysis. *The Journal of Biological Chemistry*, **292**(11): 4469–4483.

Nagaraj R, Sharpley MS, Chi FT, et al. 2017. Nuclear localization of mitochondrial TCA cycle enzymes as a critical step in mammalian zygotic genome activation. *Cell*, **168**(1): 210–223.11.

Qian C, Zhou MM. 2006. SET domain protein lysine methyltransferases: structure, specificity and catalysis. *Cellular and Molecular Life Sciences: CMLS*, **63**(23): 2755–2763.

Sfakianoudis K, Maziotis E, Karantzali E, et al. 2021. Molecular drivers of developmental arrest in the human preimplantation embryo: a systematic review and critical analysis leading to mapping future research. *International Journal of Molecular Sciences*, **22**(15): 8353.

Shao JL, Shi TZ, Yu H, et al. 2021. Cytosolic GDH1 degradation restricts protein synthesis to sustain tumor cell survival following amino acid deprivation. *The EMBO Journal*, **40**(20): e107480.

Sozen B, Can A, Demir N. 2014. Cell fate regulation during preimplantation development: a view of adhesion-linked molecular interactions. *Developmental Biology*, **395**(1): 73–83.

Sun MH, Jiang WJ, Li XH, et al. 2023. ATF6 aggravates apoptosis in early porcine embryonic development by regulating organelle homeostasis under high-temperature conditions. *Zoological Research*, **44**(5): 848–859.

Sunthankar KI, Jenkins MT, Cote CH, et al. 2022. Isocitrate dehydrogenase mutations are associated with altered IL-1β responses in acute myeloid leukemia. *Leukemia*, **36**(4): 923–934.

Tischler J, Gruhn WH, Reid J, et al. 2019. Metabolic regulation of pluripotency and germ cell fate through α-ketoglutarate. *The EMBO Journal*, **38**(1): e99518.

Wang LY, Li ZK, Wang LB, et al. 2020. Overcoming intrinsic H3K27me3 imprinting barriers improves post-implantation development after somatic cell nuclear transfer. *Cell Stem Cell*, **27**(2): 315–325. e5.

Wang W, Wang YJ, Liu YF, et al. 2023. Polymorphism and expression of *GLUD1* in relation to reproductive performance in Jining Grey goats. *Archives Animal Breeding*, **66**(4): 411–419.

Xiang JZ, Xing Y, Long CS, et al. 2020. Fatty acid metabolism as an indicator for the maternal-to-zygotic transition in porcine IVF embryos revealed by RNA sequencing. *Theriogenology*, **151**: 128–136.

Xu Y, Zhang Y, García-Cañaveras JC, et al. 2020. Chaperone-mediated autophagy regulates the pluripotency of embryonic stem cells. *Science*, **369**(6502): 397–403.

Zernicka-Goetz M, Morris SA, Bruce AW. 2009. Making a firm decision: multifaceted regulation of cell fate in the early mouse embryo. *Nature Reviews Genetics*, **10**(7): 467–477.

Zhang TR, Zheng YY, Kuang TY, et al. 2022. Arginine regulates zygotic genome activation in porcine embryos under nutrition restriction. *Frontiers in Veterinary Science*, **9**: 921406.

Zhang ZZ, He CJ, Zhang L, et al. 2019. Alpha-ketoglutarate affects murine embryo development through metabolic and epigenetic modulations. *Reproduction*, **158**(2): 123–133.

Zhou C, Wang YZ, Zhang JC, et al. 2019. H3K27me3 is an epigenetic barrier while KDM6A overexpression improves nuclear reprogramming efficiency. *The FASEB Journal*, **33**(3): 4638–4652.

Zhou WJ, Niu YJ, Nie ZW, et al. 2020. Nuclear accumulation of pyruvate dehydrogenase alpha 1 promotes histone acetylation and is essential for zygotic genome activation in porcine embryos. *Biochimica et Biophysica Acta (BBA) - Molecular Cell Research*, **1867**(4): 118648.